CIUSuite 2: Next-Generation Software for the Analysis of Gas-phase Protein Unfolding Data

Daniel A. Polasky, Sugyan M. Dixit, Sarah M. Fantin, and Brandon T. Ruotolo*

University of Michigan Department of Chemistry, Ann Arbor, Michigan 48109, United States.

ABSTRACT: Ion mobility-mass spectrometry (IM-MS) has become an important addition to the structural biology toolbox, but separating closely related protein conformations remain challenging. Collision induced unfolding (CIU) has emerged as a valuable technique for distinguishing iso-crossectional protein and protein complex ions through their distinct unfolding pathways in the gas phase. The speed and sensitivity of CIU analyses, coupled with their information-rich datasets, have resulted in the rapid growth of CIU for applications, ranging from the structural assessment of protein complexes to the characterization of biotherapeutics. This growth has occurred despite a lag in the capabilities of informatics tools available to process the complex datasets generated by CIU experiments, resulting in laborious manual analysis remaining commonplace. Here, we present CIUSuite 2, a software suite designed to enable robust, automated analysis of CIU data across the complete range of current CIU applications and to support the implementation of CIU as a true high-throughput technique. CIUSuite 2 uses statistical fitting and modeling methods to reliably quantify features of interest within CIU datasets, particularly in data with poor signal quality that cannot be interpreted with existing analysis tools. By reducing the signal-to-noise requirements for handling CIU data, we are able to demonstrate reductions in acquisition time of up to two orders of magnitude over current workflows. CIUSuite 2 also provides the first automated system for classifying CIU fingerprints, enabling the next generation of ligand screening and structural analysis experiments to be accomplished in a high-throughput fashion.

Native mass spectrometry (MS) has become a widespread technique in structural biology due to its ability to preserve noncovalently associated protein-protein and protein-ligand contacts and determine the stoichiometry and connectivity of these interactions.[1–3] The coupling of ion mobility to mass spectrometry (IM-MS) provides molecular shape information in addition to ion mass and charge, which has proven invaluable in interrogating complex biomolecular structures.[4,5] Native IM-MS has seen dramatic growth in recent years, with applications in biotherapeutic characterization[6] and drug discovery,[7] joining more traditional analyses of protein complex structure and stoichiometry. A significant challenge in IM-MS is the separation of closely related protein conformations, as biologically relevant conformational variations often occur beyond the resolution limits of modern IM instrumentation. However, gas-phase activation provides a powerful approach to probe these subtle structural differences by assessing the resulting pattern of intermediate structural families produced from collisionally heating gas-phase protein ions. Early collision induced unfolding (CIU) experiments utilized this approach to differentiate charge-driven and disulfide bonding variations in small proteins.[8] Subsequent CIU work uncovered different ligand-based stabilization mechanism in mutant TTR forms not detectable by IM-MS alone by introducing fingerprint plots that have now become a widespread analysis framework for such data.[9]

Since these early reports, CIU has seen rapid growth as such data have provided valuable approaches for a wide range of applications across the biological and pharmaceutical sciences. The characterization of protein structure and dynamics, one of the original driving forces behind the development of CIU, remains a highly active area. Several groups have used comparative CIU of protein variants to determine the importance of specific residues, domains, and post-translational modifications on the structure and function of biomolecules.[10–14] CIU has been used to rapidly probe the details of protein structure in response to solution and gas-phase stimuli.[15–20] CIU experiments have also been used to determine the orientation of ubiquitin non-covalent dimers through comparisons with various covalently linked dimers[21,22] as well as assess the domain-specific unfolding of gas-phase serum albumins.[23] Many reports have described using CIU to assess ligand binding to a variety of protein targets[9,24] in an effort to build information-rich small molecule screening platforms. CIU can be used as an analogue to stability shift assays commonly carried out in solution, as differences in gas-phase stabilities can offer similar information for unpurified samples at lower concentrations and potentially resolve intermediate transitions that may be missed in low resolution binding assays.[25–27] Others have leveraged the detailed information provided by CIU to characterize the cooperativity,[28] binding location,[29] and the allostery of ligand binding events within proteins.[30,31] CIU has also been developed into a versatile tool for the characterization of biotherapeutic antibodies.[32] For example, CIU has proven to be highly sensitive to the presence of immunoglobulin isoforms,[33] differences in glycosylation and disulfide bonding patterns,[34] antibody-drug conjugation patterns,[35] and different binding epitopes.[36] Its relative sensitivity and speed when compared to other biophysical probes has led to the deployment of CIU in broad comparisons of biosimilar therapeutics.[37–39] Finally, CIU shows promise in the context of membrane proteins,[40–43] where such data has already proven critical in revealing some of the structural consequences of off-target drug binding.[44]

Many of the CIU studies discussed above utilized manual analysis for all or part of their CIU data processing. A number of software packages are available to perform specific analytical tasks related to CIU data processing[42,45–48], and while they provide valuable capabilities, widespread adoption and use of software for processing of CIU data is still emerging. With CIUSuite 2, we combine additional capabilities for data processing not currently available in any software package, such as noise removal via Gaussian fitting and advanced classification of CIU data, with the integration of many capabilities into a single platform with a high degree of automation.

One of the most common outputs of CIU experiments is the accelerating voltage necessary to convert fifty percent of a compact protein form into an energetically adjacent extended state, sometimes termed a "CIU50" value. CIU50s have been used extensively to assess protein-ligand binding[25–28] and the stability of domains within larger protein constructs.[11,12,14,15,18,34] The Pulsar software package uses feature models to fit CIU50 values,[42] but requires manual annotation of the features prior to analysis. Other packages, including the original CIUSuite[45] and Benthesikyme,[47] annotate CIU features but lack an automated method to fit CIU50s. Another common output involves the root mean squared deviation (RMSD) analysis of CIU data, which is currently supported by several software packages[45,48] and has proven a useful approach to detect quantitative differences in CIU fingerprints. RMSD analysis of CIU data is highly sensitive to chemical noise and to overall fluctuations in signal intensity because all differences between datasets are included in quantification. RMSD is effectively an ensemble measurement of all differences between fingerprints, which can obscure the contributions of individual changes in complex datasets. In practice, extensive signal averaging is often used to overcome some of the noise-related limitations in RMSD analyses of CIU data, but this substantially limits the throughput of such experiments.

To address these challenges, we have developed CIUSuite 2, a software package that utilizes established fitting and statistical methods to enable the robust quantitation of CIU data across a broad range of CIU applications and analysis types, especially for enabling the analysis of low intensity CIU datasets. CIUSuite 2 extracts CIU50 values through a combination of improved feature detection and fits to logistic (sigmoid) curves that describe CIU transitions, enabling the fully automated and robust analysis of protein stabilities. By directly fitting features of interest, the signal-to-noise (S/N) ratios required for reliable analyses are reduced dramatically. These improved capabilities have, for example, enabled us to generate nearly identical output values from CIU data collected in 60-fold less time than previously published results. CIUSuite 2 significantly improves CIU fingerprint classification using linear discriminant analysis and support vector machines to enable next-generation high-throughput screening experiments. Finally, by modeling CIU data as mixtures of Gaussian functions, we are able to remove chemical noise and enable advanced feature detection within CIU datasets, producing robust analysis workflows for challenging CIU datasets. We have developed these algorithms with input from ongoing CIU projects that involve the assessment of biotherapeutic antibodies, membrane protein lipid binding events, protein-ligand interactions, and multiprotein complexes in an effort to provide a valuable set of quantitative tools for the broadest possible range of CIU applications. These capabilities are packaged into a user-friendly graphical interface that supports automated, high-throughput processing of large numbers of CIU datasets. CIUSuite 2 supports data collected on any IM-MS platform, and automated converters from vendor-specific data formats to the text file input needed for CIUSuite 2 are available. Finally, CIUSuite 2 is a fully open-source software package and designed to be modular and readily extensible for researchers wishing to modify its capabilities for any CIU application.

Methods

Experimental Section. Translocator Protein (TSPO) was purified and expressed using established protocols.[49] All lipids purchased from Avanti Polar Lipids (Alabaster, AL). Ammonium acetate and Octyl β-D-glucopyranoside (OG) were purchased from Sigma Aldrich (St. Louis, MO). All CIU data was collected using a Synapt G2 HDMS IM-Q-ToF mass spectrometer (Waters, Milford, MA). Intact protein ions were generated using a direct infusion nESI source in positive mode. Glycosylated antibody data were collected as described previously.[34] Briefly, enzymes were used to cleave at specific glycan residues from an antibody standard (SILuLite SigmaMAb Universal Antibody Standard human (product number: MSQC4), Sigma Aldrich, St. Louis, MO) to leave glycans of known molecular weight attached to the antibody, which was then buffer exchanged (Micro Biospin6 spin columns (Bio-Rad, Hercules, CA)) into 100 mM ammonium acetate and analyzed by IM-MS. TSPO was buffer and detergent exchanged simultaneously from 5 mM Tris, 150 mM NaCl , 0.20% DM, pH 8.0 to 40 mM OG , 200 mM ammonium acetate, pH 8.0 using 100kDa Amicon Ultra-0.5 Centrifugal Filter Units (MilliporeSigma, Burlington, MA). Lipid binding studies were performed following established protocols.[50] Instrument settings were tuned to completely remove the micelle prior to IM separator, including source temperature (40° C), helium cell gas flow (100 mL/min), and sampling cone (120 V). All CIU analyses were performed by increasing the trap collision voltage in a stepwise manner from 5 – 200 V (antibodies) or 50 – 150 V (membrane proteins) in 5 V increments.

Raw Data Extraction. Raw data was converted from Waters .raw format to a text-based format ("_raw.csv", as described previously)[45] using TWIMExtract.[51] Briefly, data from the *m/z* range corresponding to a single protein charge state was summed across the *m/z* and IM drift time dimensions to generate a series of collision voltage resolved IM datasets. For those analyses that compared different instrument acquisition times, data was summed across an indicated subset of the total acquisition time at each collision voltage. Extracted profiles are concatenated by TWIMExtract into a single _raw.csv file that serves as the input to CIUSuite 2. Raw data conversion is in development for the Agilent .d IM-MS data format. Similar converters for any additional formats (for example, an open IM-MS data format if one is developed) can be added as needed.

CIUSuite 2 Overview. CIUSuite 2 was developed in Python 3.5 utilizing the SciPy ecosystem[52,53], including NumPy,[54] Matplotlib,[55] and Scikit-learn.[56] The graphical user interface was developed using the Pygubu GUI builder (https://github.com/alejandroautalan/pygubu).

Analysis of CIU data begins by importing any number of _raw.csv (text) format files. Each file (CIU dataset) undergoes smoothing and normalization. A 2D Savitzky-Golay filter of user-specified size is the default recommended setting; how-

ever, users may also select a 1D Savitzky-Golay filter of variable size or no smoothing as options. Additional pre-processing

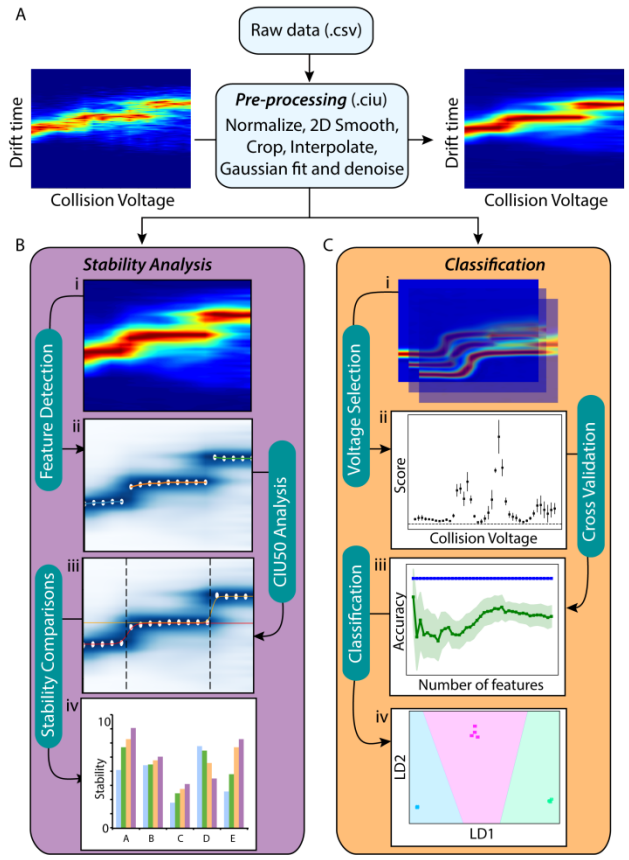

Figure 1. CIUSuite 2 overview. (A) Import of raw data from text (.csv) format and data preprocessing. (B) Stability analysis ("CIU50") workflow: i) loading of preprocessed CIU datasets, ii) detection of features, iii) logistic function fitting to determine CIU50 value(s), and iv) comparison of CIU50 values among multiple datasets. (C) Classification workflow: i) Assignment of CIU training data into classes, ii) Selection of voltages most capable of differentiating classes, iii) Cross validation for model selection, and iv) Use of the selected model to perform LDA and build a SVM for classification. The capabilities illustrated here are not intended to provide a comprehensive walkthrough of CIUSuite 2 capabilities.

options are available in CIUSuite 2, including cropping, interpolating (resampling) data along one or both axes, and averaging multiple datasets. Once this pre-processing is complete, a ".ciu" file (a serialized file created with Python's pickle module to store the CIU data and the results of any processing) is created (Figure 1A). An RMSD comparison module, similar to the one provided in the original CIUSuite, is included in CIUSuite 2, offering the ability to compare individual files or groups of files to generate pairwise RMSD values. All other analysis functions described below are unique to CIUSuite 2.

Stability Shift ("CIU50") Analysis. To determine quantitative stability values from CIU datasets, a series of processing and modeling steps is performed (Figure 1B). First, features in the dataset are detected by grouping observed drift time peaks that are present across multiple collision voltages (Figure 1B, ii). The tolerances from median drift times, as well as the number of stable collision voltages required to define a feature, can be user-adjusted. Following feature detection, the transition region between features is modeled as a logistic (generalized sigmoid) function (Figure 1B, iii, text S5). The logistic function parameters describe the lower and upper asymptotes (centroid drift times of the features before and after the transition), the steepness of the transition, and its midpoint voltage, which we term the "CIU50" value. Specifically, we define the CIU50 as the voltage at which 50% of a relatively compact state of the protein transitions to a more extended one, making it the effective midpoint between two adjacent features on a CIU fingerprint. An arbitrary number of CIU datasets can be fit in a single CIUSuite 2 analysis, enabling high-throughput analyses and comparisons of stability values for all transitions detected across many CIU fingerprints (Figure 1B, iv).

Classification. In an effort to further improve our ability to differentiate CIU fingerprint data, we developed a new classification workflow capable of sorting CIU datasets into groups using robust statistical methods. Briefly, a classification scheme is built based on training datasets from each group. First, our workflow implements a univariate feature selection (UFS) method based on an analysis of variance (ANOVA) F-test[57] to assess the significance of activation energies capable of differentiating CIU fingerprints (Scheme S1). We iterate over all possible combinations of a training dataset in order to obtain the mean and standard deviation of $-\log_{10}$(p value) which serves as the score for each collision voltage (Figure 1C, ii). Second, we employ a "leave one out" cross-validation scheme[58] that examines the accuracy of classification, which is comprised of a linear discriminant analysis[59] (LDA) step followed by support vector machine[60] (SVM) classification of the linear discriminants, using subsets of CIU data from collision voltages in decreasing order relative to the score assigned during UFS analysis (Figure S2). This enables optimal selection of collision voltages to use for the resulting model and can be used to detect under- or over-fitting in the final model selected (Figure 1C, iii). Finally, classification is performed on the model dataset with the optimized set of collision voltages, dividing the linear discriminant space into "decision regions" corresponding to the provided groups (Figure 1C, iv). The resulting classification scheme can then be used to evaluate "unknown" CIU datasets (not used in training) to predict the class and probability for each unknown. We have also included a 'manual' classification mode, where users can select any number of specific collision voltages to build a classification model. This is particularly helpful in scenarios where the accuracy observed in the cross-validation step is unacceptably low.

Gaussian Fitting and Automated De-noising. An optional Gaussian-fitting module enables modeling of the observed IM arrival time distribution at each collision voltage as a sum of Gaussian functions in order to provide a method for automated noise removal in complex datasets. An initial curve fitting[52] is performed to generate high quality initial values prior to a primary analysis run by fitting a single peak to the arrival time distribution and adding peaks until the fit to the observed data (R^2) exceeds 0.99. Fitting can be performed in both "no de-noising" and "denoising" modes to model a noise-free arrival time distribution or remove chemical noise, respectively. In each mode, the primary fitting run samples a range of Gaussian components (peaks) and scores each by its goodness of fit (R^2), peak width, and degree of overlap amongst its protein components. To perform a fit, Gaussian peak models for each component are assembled and fit to the arrival time data using LMFit.[61] In denoising mode, the IM peak width of each Gaussian feature is used to distinguish between protein and non-protein components (Text S6). The highest scoring fit at

each collision voltage is then taken for further evaluation, such as feature detection, CIU50 analysis, and classification workflows. The denoising workflow allows for the removal of chemical noise or other variability from CIU data prior to analysis, improving quantitative results (see below). Gaussian fit data can also be uploaded in a text format, enabling the use of other Gaussian fitting programs for CIU data as an alternative data input into CIUSuite 2. Data imported in this way can be analyzed using all of the tools described above.

Results and Discussion

CIU Stability Shift Analysis. Assessing a shift in the gas-phase stability of a protein or protein complex in response to some stimulus is one of the most common applications of CIU, but current methods lack the ability to return robust quantitative values for complex or low-intensity datasets. Previous work from our laboratory has utilized RMSD analysis to detect a strong correlation between CIU fingerprint data and single-sugar changes in the glycans attached to intact monoclonal antibodies (mAbs), as generated through enzymatic reactions (Figure 2A).[34] While the capability to detect such subtle differences in glycan structure within a 150 kDa protein is potentially enabling for mAb development, the length of time required to generate the data necessary to accurately quantify the above-described trends may make the adoption CIU technology for mAb assessments where rapidity is a requirement challenging. For example, in order to collect our previously reported glycoform-resolved mAb CIU dataset,[34] 60 seconds of data was summed at each of 40 collision voltages probed (5 – 200 V) across 6 glycoforms in triplicate, for both intact mAbs and Fc fragments, resulting in a total acquisition time of approximately 24 hours. Because the quantitative comparison of each glycoform relied on a total RMSD analysis of each CIU fingerprint collected, minor fluctuations in signal intensity and chemical noise can dramatically influence the values extracted. In our previous report,[34] we elected to employ extended signal averaging in order to reduce the impact of such variations, at the cost of acquisition speed.

CIUSuite 2 directly models the transitions between features of CIU fingerprints, enabling the direct assessment of stability shifts without interference from other sources of variability or noise. Since our previously-reported RMSD differences largely arise from a shift in the stability of the second feature in the CIU fingerprints recorded,[34] we fit this transition using CIUSuite 2 in order to generate a CIU50 value for each glycoform we studied previously (Figure 2B). Critically, because only the transition between the two features is used to extract correlations between sugar structures and CIU responses, the S/N ratios required for the precise assessments of such correlations are far lower than with our previous RMSD method. To demonstrate the speed improvement this affords, we extracted sub-sections of the original raw data corresponding to 1 second (a single scan collected by the instrument), 5 seconds, 15 seconds, 30 seconds, and the full 60 seconds of ion signal used in the original analysis. The S/N ratio observed in the 1-second data is approximately 60-fold lower than the full 60 seconds as expected, but the fit for the resulting logistic function that defines the CIU50 values extracted remains high quality, as shown in Figure 2B. Plotting the observed CIU50 value for each glycoform as a function of signal collection time demonstrates that there is essentially no difference (less than 0.5 V) between the results obtained using any amount of

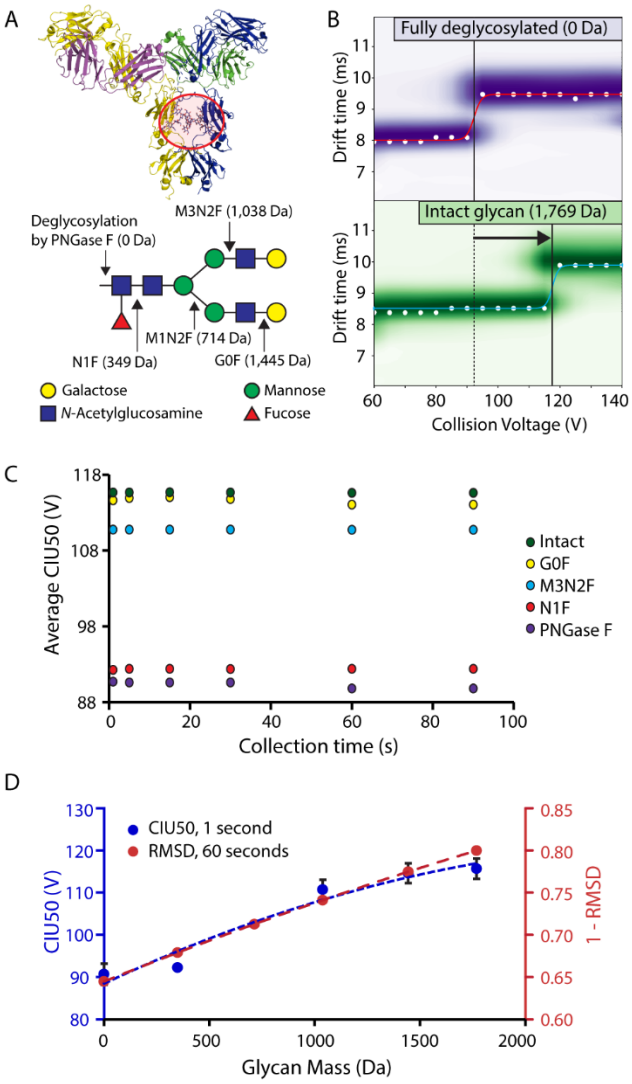

Figure 2. CIU50 analysis mAb glycoforms using CIUSuite 2. (A) Enzymatic reactions were used to produce glycans of varying size (cleavage site indicated by arrows), as described previously.[34] (B) CIU transition region shown for intact and fully deglycosylated mAbs. Larger glycans stabilize the transition between CIU features. (C) CIU50 values fit for each mAb glycoform plotted as a function of signal collection time for individual collision voltage values. Minimal variation is observed across the collection time axis, indicating that faster data acquisition is possible without affecting CIU50 values. (D) Plot of either CIU50 values from 1 s of data (blue) or previously published[34] RMSD using 60 s of data (red), against masses of mAb-attached glycans for each sample analyzed.

signal averaging probed here (Figure 2C). As such, we can reconstruct our previous correlation between CIU response and glycan mass using only 1 second of our original data (Figure 1D). The curves have similar slopes, indicating a similar glycoform sensitivity, though some variation as fundamentally different quantities different quantities are extracted from the data in the two approaches compared. Importantly, since our CIUSuite 2 method requires only 1 second of signal averaging at each collision voltage, we can reduce our total data collection time by 60-fold, resulting in a total of 24 minutes needed to quantify the same trend with equivalent precision as described in our previous report.[34]

Furthermore, we estimate that the S/N ratio of the 1-second data is still far greater (on the order of 10^4) than is required for accurate fitting, indicating that greater reductions in acquisi-

tion time are possible with shorter (sub-second) instrument scans.

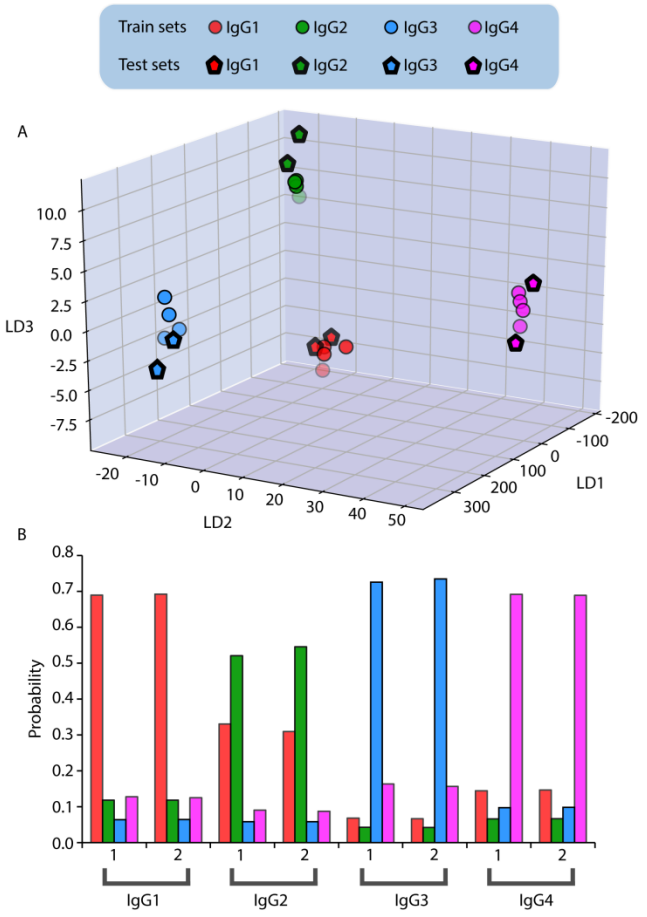

Figure 3. Classification of different IgG standards. (A) LDs for both training (filled circle) and test (filled pentagon) datasets corresponding to IgG1 (red), IgG2 (green), IgG3 (blue), and IgG4 (magenta) subclasses are well separated into clusters in three-dimensional space, defined by LD1, LD2, and LD3 axes. (B) Probabilities associated with each replicate (labeled as 1 and 2) in terms of categorizing the CIU data into different IgG groups. Each dataset is correctly assigned to its respective IgG subclass.

By directly modeling the relevant parts of a fingerprint, CIUSuite 2 is thus able to dramatically improve the speed of CIU analyses, vastly enhancing the throughput of CIU analyses.

Classification of CIU data. The unfolding pathway of gas-phase protein ions has been observed to be sensitive to changes in protein structure that remain too subtle to detect using IM-MS alone.[23,45] As such, CIU fingerprints have been deployed as means to classify protein structural states that result from changes in post-translational modifications, sequence variation, and ligand binding.[31,45] For example, recent reports have demonstrated robust CIU classification schemes capable of differentiating allosteric and active site competitive kinase inhibitors,[31] as well as binding event across two remote sites associated with transcriptional regulation.[62] However, a lack statistical methods capable of sorting of unknown CIU data against known categories or of sorting between more than two separate categories has proven to be an impediment in advancing such experiments beyond proof-of-concept demonstrations. In CIUSuite 2, we have implemented a classification workflow that uses rigorous statistical methods to generate classifying schema from known fingerprints that allows for facile evaluation of unknown samples against these schema for rapid sorting.

Data shown in Figure 3 displays an example implementation of our classification workflow, utilizing CIU data for immunoglobulin G (IgG) standards acquired across IgG1, IgG2, IgG3, and IgG4 subclasses. Each of our IgG CIU datasets contained four replicates, which we subdivided evenly into both training and test data in order to evaluate our approach. Of the forty collision voltages acquired for each CIU dataset, only a few were found to be highly differentiating between classes by UFS, with 85 V having the maximum score (Figure S3E). This voltage is near the value required for the first CIU transition for each IgG subclass (Figures S3A – S3D). Cross-validation of UFS results revealed a classification accuracy 92.2% using only the CIU data isolated at 85 V, and decreases as additional CIU data is added (Figure S3F). Thus, our algorithm selected CIU data acquired at 85 V automatically in order to build a classification scheme. Figure 3A shows the three-dimensional plot of linear discriminants (LDs) constructed using this data, which groups IgG CIU data into well-separated clusters. Furthermore, test data clustered correctly in all cases using this classification scheme (pentagons, Figure 3A). We further used CIUSuite to compute the probability of each test dataset clustering into each IgG subclass (Figure 3B), finding that each dataset was classified correctly with probability values ranging from 0.52 – 0.73 (Table S4). In general, our CIU classification workflow is generalizable, rapidly processing data in an automated fashion and accommodating any grouping scheme.

Classifying Noisy, Low Intensity CIU Data. While many existing tools are capable of analyzing high S/N data, low intensity CIU data containing significant amounts of chemical noise is exceptionally challenging to extract quantitative data from using current analysis paradigms. Membrane protein CIU data presents many of these challenges, as it frequently contains low-intensity protein ion signals, overlapped with intense chemical noise derived from detergents or other solubilizing agents, and is collected in a mode that thwarts typical tandem MS based CIU workflows.[50,63] The feature detection and CIU50 functions of CIUSuite 2 were designed to extract reliable quantitative values from such datasets. Figure 4 illustrates the capabilities of CIUSuite 2 for such applications using data acquired for TSPO, a 36 kDa mitochondrial transmembrane protein dimer associated with benzodiazepine binding and cholesterol transport. Our feature detection workflow in CIUSuite 2 considers only the most intense IM peaks observed, and thus acts as an amplitude filter, removing such detergent and lipid based chemical noise signals from subsequent analysis steps. CIU50 values can then be fit to the observed transitions between features without interference (Figure 4A), so long as protein signals comprise the most intense peaks in the IM data analyzed. If this is not the case, automated noise removal can be employed prior to fitting (see below).

CIU has been used to characterize lipid binding to membrane proteins in order to assess stability shifts in the resulting complexes.[42–44] Such data have been further used to distinguish between biologically relevant and nonspecifically associated lipids in membrane proteins.[41] Counterintuitively, such assessments are often more straightforward to perform for larger proteins and complexes, as they appear at m/z and IM drift

times that are frequently less contaminated by chemical noise. Since TSPO is a relatively small membrane protein complex, it is an exceptionally difficult target for CIU analysis. Preliminary

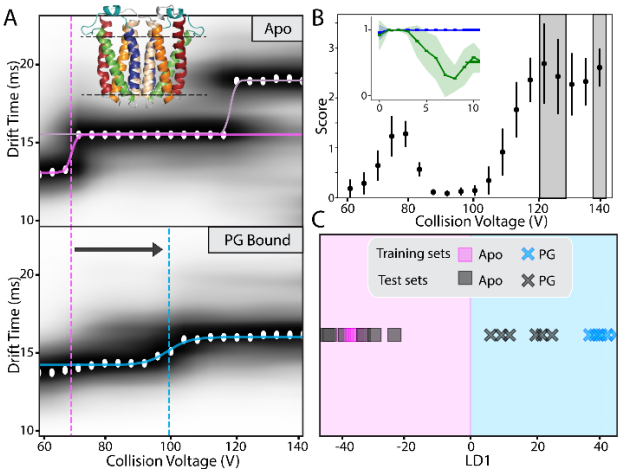

Figure 4. CIU50 analysis and classification TSPO-lipid complexes. (A) Feature fitting ignores low abundance chemical noise and CIU50 analysis reveals a stability shift associated with PG-bound TSPO. (B) Three voltages (120 V, 125 V, and 140 V) are used to construct a classification scheme from apo and PG-bound TSPO training sets, the inset shows a cross-validation plot indicating a high accuracy classification. (C) Additional test data sets are correctly assigned to apo (pink) or PG-bound (blue) TSPO.

screening of TSPO-lipid complexes revealed certain lipids, such as phosphatidylglycerol (PG), that significantly stabilize the protein so that CIU transitions appear distorted relative to apo protein data, making the extraction of CIU50 values even more challenging.[64] We used the CIU50 module within CIUSuite 2 to fit these highly stabilized TSPO-PG transitions, allowing us to quantify stability imparted by lipid binding (Figure 4A, lower panel). While this analysis provides high quality stability shift values, high-throughput CIU protocols require the rapid classification of ligands based on fingerprint data. To that end, we classified PG-bound and apo TSPO CIU signatures using CIUSuite 2. By using three replicates each of apo and lipid bound data to build the classification scheme, we identified 120 V, 125 V, and 140 V as the most differentiating collision voltage values in our dataset (Figure 4B). For validation of our classification scheme, four data sets that were not part of the training dataset were input as unknowns, and all were correctly classified (Figure 4C). While it is clear that mass analysis alone could be used to identify PG bound and apo TSPO, these results illustrate a classification outcome that is exceptionally challenging to achieve using current CIU analysis tools.

Gaussian Fitting and Automated Denoising. The feature detection and CIU50 analyses presented in Figure 4A enable the examination of CIU data containing a modest amount of chemical noise by employing a simple high-pass amplitude data filter and relying upon the presence of high-intensity protein signal. In many cases, however, protein signals are overlapped with chemical noise at intensity comparable to or exceeding that of the protein, rending a high-pass filter approach ineffective. In such cases, quantified values extracted from CIU data exhibit reduced accuracy, reproducibility, and in some cases may be entirely unrecoverable. For example, the TSPO CIU data shown in Figure 5A contains chemical noise

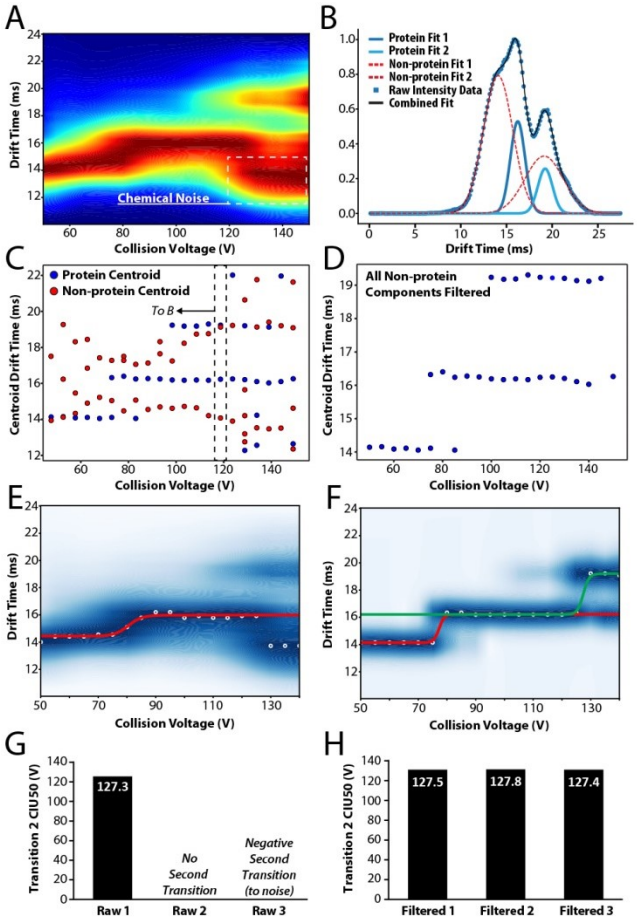

Figure 5. Automated de-noising of membrane protein CIU data using Gaussian fitting. (A) TSPO CIU fingerprint with chemical noise preventing analysis of the final CIU transition observed (collision voltage >120 V). (B) Example mixed-model Gaussian fit produced from selected data from A. Protein components (blue) exhibit widths within pre-defined tolerances while non-protein components (red) are broader. (C) Plot protein (blue) and non-protein (red) Gaussian fit centroids from fingerprint shown in (A). Horizontal arrays of blue dots indicate stable protein conformations (features). The region corresponding data displayed in panel B is marked. (D) Removal of non-protein components after denoising results in a centroid plot absent of the identified noise features. (E) CIU50 fitting result prior to Gaussian denoising. The second protein CIU transition is missed due to chemical noise. (F) CIU50 fitting of the same dataset as shown in E after denoising, illustrating robust recovery of both CIU transitions. (G) Histogram of CIU50 values extracted from 3 replicate datasets prior to denoising, illustrating inconsistent results. (H) Histogram of CIU50 values extracted from the same dataset as shown in panel G following denoising are highly reproducible.

that achieves greater intensity values than the detected protein ion signal at collision energies above 120 V, effectively preventing CIU50 analysis from recognizing the second protein CIU transition, which appears at 130 V. In order to surmount such signal processing difficulties, have developed a Gaussian peak-fitting module within CIUSuite 2 that provides automated noise removal from CIU fingerprints. Other CIU analysis packages have performed Gaussian fits of CIU data for feature detection,[47] however, this approach has not been previously applied to removal of noise components from CIU data. IM peaks corresponding to protein ions exhibit a range of peak widths produced primarily by ion diffusion and conformational heterogeneity effects[65–67] Thus, the likely range of IM

peak widths for protein signals can be utilized as a noise filter for CIU analysis, where Gaussian fits corresponding to features that exceed such a width tolerance are identified as noise and subtracted from the final fingerprint. Fitting is performed using two different types of components: protein components (e.g. the blue traces in Figure 5B), which are Gaussian functions constrained to a narrow distribution of peak widths, and non-protein components (e.g. the red dashed lines in Figure 5B), which are allowed to have any width substantially larger than the upper width limit allowed for protein components. This approach intrinsically filters resulting fit results, allowing noise components to be removed after the fitting is complete. Figure 5C shows the results of this automated fitting approach for phosphatidylcholine bound-TSPO CIU data displayed in Figure 5A by plotting the peak centers determined for each protein component in blue and those determined for each non-protein component in red. Three clear features, or sets of protein peak centers that appear at consistent arrival times, can be observed in the protein data, resembling a typical TSPO CIU fingerprint when the broader features are subtracted from the dataset (Figure 5D). This denoised data can then be analyzed with any of the workflows available in CIUSuite 2, including the CIU50 determination and classification modules. CIU50 analysis of the denoised dataset allows for the recovery of the second TSPO CIU transition following the removal abundant chemical noise (Figure 5F). Removing chemical noise can greatly improve the accuracy and reproducibility of CIU analyses, as in the replicate CIU50 analyses shown in Figures 5G, H. Analysis of the raw TSPO CIU data results in adequate fits the second CIU transition in only one out of three datasets, missing the transition in the second replicate (pictured in Figure 5E) and fitting a "negative" transition (an apparent shift from longer to shorter IM drift times) to the chemical noise observed, (Figure 5G). In contrast, all three replicates can be reproducibly fit following Gaussian denoising, producing CIU50 values that vary by less than 0.4 V across all three replicates (Figure 5H).

The automated removal of chemical noise or other interfering signals from CIU data thus enables the analysis CIU datasets that would be challenging to accomplish using current tools, while requiring minimal user intervention. Protein and noise components can be distinguished based on their differential peak widths, allowing such noise to be directly subtracted from CIU fingerprints. Combined with CIU50 analysis and classification workflows, Gaussian denoising represents a substantial enhancement to the CIU signal processing toolbox.

Conclusions

CIU experiments generate complex datasets containing rich protein structure information. CIUSuite 2 provides a framework, built upon established statistical methods, for extracting key information from CIU data in a robust, automated fashion. Furthermore, CIUSuite 2 is designed to support a broad range of existing CIU applications, including the analysis of noise-contaminated membrane proteins and high-throughput screening. Our improvements to the automation CIU signal processing and acquisition speed point towards the next generation of CIU workflows, where full CIU fingerprints are collected in seconds and on-the-fly data reduction enables the rapid generation of classification schema. With support from autosampling devices, the potential exists to generate and analyze orders of magnitude more CIU data per unit time than currently possible. The ability to generate such large datasets would likely aide in answering fundamental questions regarding the relationship between solution and gas-phase stabilities and structures, while simultaneously providing a platform for rapid structural assessments of biotherapeutics and pharmaceutically relevant protein complexes. CIUSuite 2 is available for download at https://sites.lsa.umich.edu/ruotolo/software/ciusuite-2/, and its source code can be found at https://github.com/RuotoloLab/CIUSuite2.

ASSOCIATED CONTENT

Supporting Information

The Supporting Information is available free of charge on the ACS Publications website.

Details of Classification univariate feature selection (UFS) and cross validation; UFS, cross validation, and test data probability results corresponding to Figure 3, details of logistic fitting for CIU50 analysis, timing benchmarks for Gaussian fitting and classification methods, and scoring functions and details for Gaussian fitting methods.

AUTHOR INFORMATION

Corresponding Author

*E-mail: bruotolo@umich.edu

ORCID

Daniel A. Polasky: 0000-0002-0515-1735
Sugyan M. Dixit: 0000-0002-6313-7974

Author Contributions

The manuscript was written through contributions of all authors. All authors have given approval to the final version of the manuscript.

Notes

The authors declare no competing financial interest.

ACKNOWLEDGMENT

TSPO protein was expressed and purified by the Ferguson-Miller group at Michigan State University. The authors thank M. W. Haskell for helpful discussions regarding Gaussian fitting and modeling, and the members of the Ruotolo lab for extensive feedback and beta testing. CIUSuite 2 development is supported by the National Science Foundation Division of Chemistry under Grants 1808541 and 1253384 (with co-funding from the Division of Molecular and Cellular Biosciences). Additional support for this project was provided by the Agilent Technologies Thought Leader Award and University Relations grant programs.

REFERENCES

(1) Leney, A. C.; Heck, A. J. R. Native Mass Spectrometry: What Is in the Name? *J. Am. Soc. Mass Spectrom.* **2017**, *28* (1), 5–13.

(2) Lössl, P.; van de Waterbeemd, M.; Heck, A. J. The Diverse and Expanding Role of Mass Spectrometry in Structural and Molecular Biology. *EMBO J.* **2016**, *35* (24), 2634–2657.

(3) Mehmood, S.; Allison, T. M.; Robinson, C. V. Mass Spectrometry of Protein Complexes: From Origins to Applications. *Annu. Rev. Phys. Chem.* **2015**, *66* (1), 453–474.

(4) Zhong, Y.; Hyung, S.-J.; Ruotolo, B. T. Ion Mobility–mass Spectrometry for Structural Proteomics. *Expert Rev. Proteomics* **2012**, *9* (1), 47–58.

(5) Lanucara, F.; Holman, S. W.; Gray, C. J.; Eyers, C. E. The Power of Ion Mobility-Mass Spectrometry for Structural Characterization and the Study of Conformational Dynamics. *Nat. Chem.* **2014**, *6* (4), 281–294.

(6) Terral, G.; Beck, A.; Cianférani, S. Insights from Native Mass

Spectrometry and Ion Mobility-Mass Spectrometry for Antibody and Antibody-Based Product Characterization. *J. Chromatogr. B Anal. Technol. Biomed. Life Sci.* **2016**, *1032*, 79–90.

(7) Bleiholder, C.; Bowers, M. T. The Solution Assembly of Biological Molecules Using Ion Mobility Methods: From Amino Acids to Amyloid β-Protein. *Annu. Rev. Anal. Chem* **2017**, *10* (1), 365–386.

(8) Shelimov, K. B.; Clemmer, D. E.; Hudgins, R. R.; Jarrold, M. F. Protein Structure in Vacuo: Gas-Phase Conformations of BPTI and Cytochrome C. *J. Am. Chem. Soc.* **1997**, *119* (9), 2240–2248.

(9) Hyung, S. J.; Robinson, C. V.; Ruotolo, B. T. Gas-Phase Unfolding and Disassembly Reveals Stability Differences in Ligand-Bound Multiprotein Complexes. *Chem. Biol.* **2009**, *16* (4), 382–390.

(10) Zhang, H.; Liu, H.; Lu, Y.; Wolf, N. R.; Gross, M. L.; Blankenship, R. E. Native Mass Spectrometry and Ion Mobility Characterize the Orange Carotenoid Protein Functional Domains. *Biochim. Biophys. Acta - Bioenerg.* **2016**, *1857* (6), 734–739.

(11) Zhao, Y.; Singh, A.; Xu, Y.; Zong, C.; Zhang, F.; Boons, G. J.; Liu, J.; Linhardt, R. J.; Woods, R. J.; Amster, I. J. Gas-Phase Analysis of the Complex of Fibroblast GrowthFactor 1 with Heparan Sulfate: A Traveling Wave Ion Mobility Spectrometry (TWIMS) and Molecular Modeling Study. *J. Am. Soc. Mass Spectrom.* **2017**, *28* (1), 96–109.

(12) Chorev, D. S.; Volberg, T.; Livne, A.; Eisenstein, M.; Martins, B.; Kam, Z.; Jockusch, B. M.; Medalia, O.; Sharon, M.; Geiger, B. Conformational States during Vinculin Unlocking Differentially Regulate Focal Adhesion Properties. *Sci. Rep.* **2018**, *8* (1), 2693.

(13) Byrne, D. P.; Vonderach, M.; Ferries, S.; Brownridge, P. J.; Eyers, C. E.; Eyers, P. A. CAMP-Dependent Protein Kinase (PKA) Complexes Probed by Complementary Differential Scanning Fluorimetry and Ion Mobility-Mass Spectrometry. *Biochem. J.* **2016**, *473* (19), 3159–3175.

(14) Jovcevski, B.; Kelly, M. A.; Aquilina, J. A.; Benesch, J. L. P.; Ecroyd, H. Evaluating the Effect of Phosphorylation on the Structure and Dynamics of Hsp27 Dimers by Means of Ion Mobility Mass Spectrometry. *Anal. Chem.* **2017**, *89* (24), 13275–13282.

(15) Chan, D. S. H.; Kavanagh, M. E.; McLean, K. J.; Munro, A. W.; Matak-Vinković, D.; Coyne, A. G.; Abell, C. Effect of DMSO on Protein Structure and Interactions Assessed by Collision-Induced Dissociation and Unfolding. *Anal. Chem.* **2017**, *89* (18), 9976–9983.

(16) Laszlo, K. J.; Munger, E. B.; Bush, M. F. Folding of Protein Ions in the Gas Phase after Cation-to-Anion Proton-Transfer Reactions. *J. Am. Chem. Soc.* **2016**, *138* (30), 9581–9588.

(17) Beynon, R. J.; Armstrong, S. D.; Claydon, A. J.; Davidson, A. J.; Eyers, C. E.; Langridge, J. I.; Gómez-Baena, G.; Harman, V. M.; Hurst, J. L.; Lee, V.; et al. Mass Spectrometry for Structural Analysis and Quantification of the Major Urinary Proteins of the House Mouse. *Int. J. Mass Spectrom.* **2015**, *391*, 146–156.

(18) Han, L.; Hyung, S. J.; Mayers, J. J. S.; Ruotolo, B. T. Bound Anions Differentially Stabilize Multiprotein Complexes in the Absence of Bulk Solvent. *J. Am. Chem. Soc.* **2011**, *133* (29), 11358–11367.

(19) Zhong, Y.; Han, L.; Ruotolo, B. T. Collisional and Coulombic Unfolding of Gas-Phase Proteins: High Correlation to Their Domain Structures in Solution. *Angew. Chemie - Int. Ed.* **2014**, *53* (35), 9209–9212.

(20) Samulak, B. M.; Niu, S.; Andrews, P. C.; Ruotolo, B. T. Ion Mobility-Mass Spectrometry Analysis of Cross-Linked Intact Multiprotein Complexes: Enhanced Gas-Phase Stabilities and Altered Dissociation Pathways. *Anal. Chem.* **2016**, *88* (10), 5290–5298.

(21) Wagner, N. D.; Russell, D. H. Defining Noncovalent Ubiquitin Homodimer Interfacial Interactions through Comparisons with Covalently Linked Diubiquitin. *J. Am. Chem. Soc.* **2016**, *138* (51), 16588–16591.

(22) Wagner, N. D.; Clemmer, D. E.; Russell, D. H. ESI-IM-MS and Collision-Induced Unfolding That Provide Insight into the Linkage-Dependent Interfacial Interactions of Covalently Linked Diubiquitin. *Anal. Chem.* **2017**, *89* (18), 10094–10103.

(23) Eschweiler, J. D.; Martini, R. M.; Ruotolo, B. T. Chemical Probes and Engineered Constructs Reveal a Detailed Unfolding Mechanism for a Solvent-Free Multidomain Protein. *J. Am. Chem. Soc.* **2017**, *139* (1), 534–540.

(24) Hopper, J. T. S.; Oldham, N. J. Collision Induced Unfolding of Protein Ions in the Gas Phase Studied by Ion Mobility-Mass Spectrometry: The Effect of Ligand Binding on Conformational Stability. *J. Am. Soc. Mass Spectrom.* **2009**, *20* (10), 1851–1858.

(25) Zhao, Y.; Singh, A.; Li, L.; Linhardt, R. J.; Xu, Y.; Liu, J.; Woods, R. J.; Amster, I. J. Investigating Changes in the Gas-Phase Conformation of Antithrombin III upon Binding of Arixtra Using Traveling Wave Ion Mobility Spectrometry (TWIMS). *Analyst* **2015**, *140* (20), 6980–6989.

(26) Nyon, M. P.; Prentice, T.; Day, J.; Kirkpatrick, J.; Sivalingam, G. N.; Levy, G.; Haq, I.; Irving, J. A.; Lomas, D. A.; Christodoulou, J.; et al. An Integrative Approach Combining Ion Mobility Mass Spectrometry, X-Ray Crystallography, and Nuclear Magnetic Resonance Spectroscopy to Study the Conformational Dynamics of A1-Antitrypsin upon Ligand Binding. *Protein Sci.* **2015**, *24* (8), 1301–1312.

(27) Zhao, B.; Zhuang, X.; Pi, Z.; Liu, S.; Liu, Z.; Song, F. Determining the Effect of Catechins on SOD1 Conformation and Aggregation by Ion Mobility Mass Spectrometry Combined with Optical Spectroscopy. *J. Am. Soc. Mass Spectrom.* **2018**, *29* (4), 734–741.

(28) Niu, S.; Ruotolo, B. T. Collisional Unfolding of Multiprotein Complexes Reveals Cooperative Stabilization upon Ligand Binding. *Protein Sci.* **2015**, *24* (8), 1272–1281.

(29) Rabuck, J. N.; Hyung, S. J.; Ko, K. S.; Fox, C. C.; Soellner, M. B.; Ruotolo, B. T. Activation State-Selective Kinase Inhibitor Assay Based on Ion Mobility-Mass Spectrometry. *Anal. Chem.* **2013**, *85* (15), 6995–7002.

(30) Beveridge, R.; Migas, L. G.; Payne, K. A. P.; Scrutton, N. S.; Leys, D.; Barran, P. E. Mass Spectrometry Locates Local and Allosteric Conformational Changes That Occur on Cofactor Binding. *Nat. Commun.* **2016**, *7*, 12163.

(31) Rabuck-Gibbons, J. N.; Keating, J. E.; Ruotolo, B. T. Collision Induced Unfolding and Dissociation Differentiates ATP-Competitive from Allosteric Protein Tyrosine Kinase Inhibitors. *Int. J. Mass Spectrom.* **2018**, *427*, 151–156.

(32) Tian, Y.; Ruotolo, B. T. The Growing Role of Structural Mass Spectrometry in the Discovery and Development of Therapeutic Antibodies. *Analyst* **2018**, *143* (11), 2459–2468.

(33) Tian, Y.; Han, L.; Buckner, A. C.; Ruotolo, B. T. Collision Induced Unfolding of Intact Antibodies: Rapid Characterization of Disulfide Bonding Patterns, Glycosylation, and Structures. *Anal. Chem.* **2015**, *87* (22), 11509–11515.

(34) Tian, Y.; Ruotolo, B. T. Collision Induced Unfolding Detects Subtle Differences in Intact Antibody Glycoforms and Associated Fragments. *Int. J. Mass Spectrom.* **2018**, *425*, 1–9.

(35) Botzanowski, T.; Erb, S.; Hernandez-Alba, O.; Ehkirch, A.; Colas, O.; Wagner-Rousset, E.; Rabuka, D.; Beck, A.; Drake, P. M.; Cianférani, S. Insights from Native Mass Spectrometry Approaches for Top- and Middle- Level Characterization of Site-Specific Antibody-Drug Conjugates. *MAbs* **2017**, *9* (5), 801–811.

(36) Huang, Y.; Salinas, N. D.; Chen, E.; Tolia, N. H.; Gross, M. L. Native Mass Spectrometry, Ion Mobility, and Collision-Induced Unfolding Categorize Malaria Antigen/Antibody Binding. *J. Am. Soc. Mass Spectrom.* **2017**, *28* (11), 2515–2518.

(37) Campuzano, I. D. G.; Larriba, C.; Bagal, D.; Schnier, P. D. Ion Mobility and Mass Spectrometry Measurements of the Humanized IgGk NIST Monoclonal Antibody. *ACS Symp. Ser.* **2015**, *1202*, 75–112.

(38) Pisupati, K.; Tian, Y.; Okbazghi, S.; Benet, A.; Ackermann, R.; Ford, M.; Saveliev, S.; Hosfield, C. M.; Urh, M.; Carlson, E.; et al. A Multidimensional Analytical Comparison of Remicade and the Biosimilar Remsima. *Anal. Chem.* **2017**, *89* (9), 4838–4846.

(39) Ferguson, C. N.; Gucinski-Ruth, A. C. Evaluation of Ion Mobility-Mass Spectrometry for Comparative Analysis of Monoclonal Antibodies. *J. Am. Soc. Mass Spectrom.* **2016**, *27* (5), 822–833.

(40) Reading, E.; Liko, I.; Allison, T. M.; Benesch, J. L. P.; Laganowsky, A.; Robinson, C. V. The Role of the Detergent Micelle in Preserving the Structure of Membrane Proteins in the

Gas Phase. *Angew. Chemie - Int. Ed.* **2015**, *54* (15), 4577–4581.
(41) Laganowsky, A.; Reading, E.; Allison, T. M.; Ulmschneider, M. B.; Degiacomi, M. T.; Baldwin, A. J.; Robinson, C. V. Membrane Proteins Bind Lipids Selectively to Modulate Their Structure and Function. *Nature* **2014**, *510* (7503), 172–175.
(42) Allison, T. M.; Reading, E.; Liko, I.; Baldwin, A. J.; Laganowsky, A.; Robinson, C. V. Quantifying the Stabilizing Effects of Protein-Ligand Interactions in the Gas Phase. *Nat. Commun.* **2015**, *6*, 8551.
(43) Liu, Y.; Cong, X.; Liu, W.; Laganowsky, A. Characterization of Membrane Protein–Lipid Interactions by Mass Spectrometry Ion Mobility Mass Spectrometry. *J. Am. Soc. Mass Spectrom.* **2017**, *28* (4), 579–586.
(44) Mehmood, S.; Marcoux, J.; Gault, J.; Quigley, A.; Michaelis, S.; Young, S. G.; Carpenter, E. P.; Robinson, C. V. Mass Spectrometry Captures Off-Target Drug Binding and Provides Mechanistic Insights into the Human Metalloprotease ZMPSTE24. *Nat. Chem.* **2016**, *8* (12), 1152–1158.
(45) Eschweiler, J. D.; Rabuck-Gibbons, J. N.; Tian, Y.; Ruotolo, B. T. CIUSuite: A Quantitative Analysis Package for Collision Induced Unfolding Measurements of Gas-Phase Protein Ions. *Anal. Chem.* **2015**, *87* (22), 11516–11522.
(46) Sivalingam, G. N.; Yan, J.; Sahota, H.; Thalassinos, K. Amphitrite: A Program for Processing Travelling Wave Ion Mobility Mass Spectrometry Data. *Int. J. Mass Spectrom.* **2013**, *345–347*, 54–62.
(47) Sivalingam, G. N.; Cryar, A.; Williams, M. A.; Gooptu, B.; Thalassinos, K. Deconvolution of Ion Mobility Mass Spectrometry Arrival Time Distributions Using a Genetic Algorithm Approach: Application to A1-Antitrypsin Peptide Binding. *Int. J. Mass Spectrom.* **2018**, *426*, 29–37.
(48) Migas, L. G.; France, A. P.; Bellina, B.; Barran, P. E. ORIGAMI: A Software Suite for Activated Ion Mobility Mass Spectrometry (AIM-MS) Applied to Multimeric Protein Assemblies. *Int. J. Mass Spectrom.* **2018**, *427*, 20–28.
(49) Li, F.; Xia, Y.; Meiler, J.; Ferguson-Miller, S. Characterization and Modeling of the Oligomeric State and Ligand Binding Behavior of Purified Translocator Protein 18 KDa from Rhodobacter Sphaeroides. *Biochemistry* **2013**, *52* (34), 5884–5899.
(50) Laganowsky, A.; Reading, E.; Hopper, J. T. S.; Robinson, C. V. Mass Spectrometry of Intact Membrane Protein Complexes. *Nat. Protoc.* **2013**, *8* (4), 639–651.
(51) Haynes, S. E.; Polasky, D. A.; Dixit, S. M.; Majmudar, J. D.; Neeson, K.; Ruotolo, B. T.; Martin, B. R. Variable-Velocity Traveling-Wave Ion Mobility Separation Enhancing Peak Capacity for Data-Independent Acquisition Proteomics. *Anal. Chem.* **2017**, *89* (11), 5669–5672.
(52) Millman, K. J.; Aivazis, M. Python for Scientists and Engineers. *Comput. Sci. Eng.* **2011**, *13* (2), 9–12.
(53) Oliphant, T. E. Python for Scientific Computing. *Comput. Sci. Eng.* **2007**, *9* (3), 10–20.
(54) Dubois, P. F.; Hinsen, K.; Hugunin, J. Numerical Python. *Comput. Phys.* **1996**, *10* (3), 262.
(55) Hunter, J. D. Matplotlib: A 2D Graphics Environment. *Comput. Sci. Eng.* **2007**, *9* (3), 99–104.
(56) Pedregosa, F.; Varoquax, G.; Gramfort, A.; Michel, V.; Thirion, B.; Grisel, O. Scikit-Learn: Machine Learning in Python. *J Mach Learn Res* **2011**, *12* (Oct), 2825–2830.
(57) Dowdy, S. M.; Wearden, S.; Chilko, D. M. *Statistics for Research*, 3rd ed.; Wiley-Interscience: Hoboken, N.J., 2004.
(58) Arlot, S.; Celisse, A. A Survey of Cross-Validation Procedures for Model Selection. *Stat. Surv.* **2009**, *4* (0), 40–79.
(59) Xanthopoulos, P.; Pardalos, P. M.; Trafalis, T. B. Linear Discriminant Analysis; Springer, New York, NY, 2013; pp 27–33.
(60) Mammone, A.; Turchi, M.; Cristianini, N. Support Vector Machines. In *Advanced Review*; Springer, New York, NY, 2009; Vol. 1, pp 283–289.
(61) Newville, M.; Ingargiola, A.; Stensitzki, T.; Allen, D. B. LMFIT: Non-Linear Least-Square Minimization and Curve-Fitting for Python. *Zenodo* **2014**.
(62) Rabuck-Gibbons, J. N.; Lodge, J.; Mapp, A.; Ruotolo, B. T. In Press. *J Am Soc Mass Spectrom*.
(63) Campuzano, I. D. G.; Li, H.; Bagal, D.; Lippens, J. L.; Svitel, J.; Kurzeja, R. J. M.; Xu, H.; Schnier, P. D.; Loo, J. A. Native MS Analysis of Bacteriorhodopsin and an Empty Nanodisc by Orthogonal Acceleration Time-of-Flight, Orbitrap and Ion Cyclotron Resonance. *Anal. Chem.* **2016**, *88* (24), 12427–12436.
(64) Fantin, S. M.; Parson, K. F.; Niu, S.; Liu, J.; Ferguson-Miller, S. M.; Ruotolo, B. T. CIU Classifies Ligand Binding Behavior of Integral Membrane Translocator Protein TSPO. *Press*.
(65) Allen, S. J.; Giles, K.; Gilbert, T.; Bush, M. F. Ion Mobility Mass Spectrometry of Peptide, Protein, and Protein Complex Ions Using a Radio-Frequency Confining Drift Cell. *Analyst* **2016**, *141* (3), 884–891.
(66) Zhou, M.; Politis, A.; Davies, R. B.; Liko, I.; Wu, K.-J.; Stewart, A. G.; Stock, D.; Robinson, C. V. Ion Mobility–mass Spectrometry of a Rotary ATPase Reveals ATP-Induced Reduction in Conformational Flexibility. *Nat. Chem.* **2014**, *6* (3), 208–215.
(67) May, J. C.; McLean, J. A. Ion Mobility-Mass Spectrometry: Time-Dispersive Instrumentation. *Anal. Chem.* **2015**, *87* (3), 1422–1436.

Authors are required to submit a graphic entry for the Table of Contents (TOC) that, in conjunction with the manuscript title, should give the reader a representative idea of one of the following: A key structure, reaction, equation, concept, or theorem, etc., that is discussed in the manuscript. Consult the journal's Instructions for Authors for TOC graphic specifications.

Insert Table of Contents artwork here